Experimental and Computational Investigation of Novel Triazole-Pyrazole Derivative as a Synthetic Corrosion Inhibitor for M-Steel in 1.0M HCl.

Nawal Setti[1,*], *Asma* Barrahi[2], *Abdellah* Elyoussfi[1,3], *Youssef* Draoui[1], *Smail* Radi[1], *Abdelkader* Zarrouk[2], and *Ali* Dafali[1,*].

[1]LCEA Laboratory, Mohammed First University, Faculty of Sciences, Oujda, Morocco.
[2]Laboratory of Materials, Nanotechnology and Environment, Faculty of Sciences, Mohammed V University in Rabat, P.O. Box. 1014, Rabat, Morocco.
[3]Applied Chemistry Team, FSTH, Abdelmalek Essaâdi University, Tetouan, Morocco.

Abstract. TzPz, a newly synthesized ethyl 2-(3-(3,5-dimethyl-1H-pyrazol-1-yl)-H-1,2,4-triazol-1-yl) ethan-ol, was evaluated as a mild steel corrosion inhibitor in 1.0 HCl environment. The synthesis objective for this type of molecule-type was to create a triazole-based molecule with a simple yet effective structure, as well as to increase the number of nitrogen donors to boost adsorption affinities at the metal surface. This investigation began with electrochemical techniques such as EIS & PDP. The results obtained suggest that TzPz is a good inhibitor, with a maximal effectiveness (91.9%) at 303 K. The inhibitory efficacy increases dramatically with increasing concentration and decreases with increasing temperature. According to electrochemical data, TzPz functions as a mixed inhibitor, and the corrosion process is controlled by charge transfer. In addition, the adsorption isotherm adheres to the Langmuir model. UV-visible spectroscopy is used to evaluate the probability of Fe-inhibitory molecule interactions. Theoretical calculations using the DFT technique were performed and discussed for the molecule TzPz in order to understand its interfacial approach and compare them to experimental data.

Keywords. Pyrazole-Triazole; M-Steel; EIS/PDP techniques; Theoretical calculation.

*Corresponding authors: Dafali2@yahoo.fr

nawalsetti@hotmail.com

1 Introduction

Heterocyclic nitrogen compounds have a significant role in the field of corrosion inhibition, particularly vis-a-vis the corrosion of a metal much used in industrial domain, namely steel. Among the various types of heterocyclic systems, triazoles and pyrazoles stand out as widely recognized and representative five-membered heterocycles[1-3]. These chemicals compounds find utility in many different applications thanks to their exceptional properties. As an effective organic inhibitor of the presence of the electron doublet on nitrogen.

Mild steel is among metals which having weak behavior towards acid environments giving rise to corrosion attack and consequently a horrible cost of industrial field[4, 5] [6].
In this paper, the inhibitor (TzPz) is examined, and Fig.1 below depicts its chemical structure.

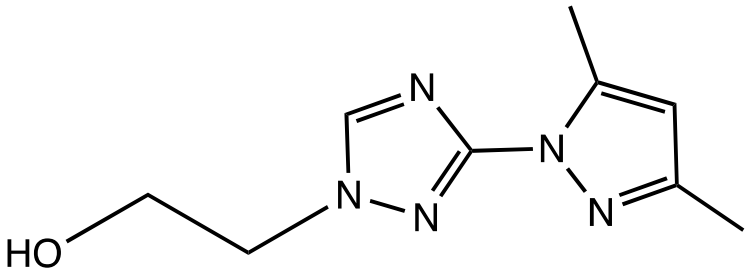

Fig.1. Molecular Structure of TzPz.

2 Experimental

2.1 Electrolyte and Materials

This experiment uses a commercial 37% HCl acid solution that has been diluted to 1M as the blank electrolyte. With the use of an electronic balance, we were able to weigh the necessary amount to make the various inhibitor concentrations. We then added the blank solution to the graduated flask then completed by the blank solution, and mix until homogeneous. Consequently, solutions with concentrations range (10^{-3} - 10^{-6}) M were prepared in order to conduct electrochemical studies. The chemical composition of the CS metal plates examined in this work is listed in table 1. CS samples are parts disc-shaped of 1 cm^2 for electrochemistry and square parts of 2.5 cm × 2.5 cm × 0.05 cm for the UV measurement, which have been polished using a range of emery paper (180 - 1200). After that, they are dried, washed with bidistilled water, submerged in a 1M HCl both with presence & absence of inhibitor concentrations.

Table 1 Chemical composition of CS.

Elements	Fer	C	Si	P	Mn	Al	S
% by mass	99.21	0.21	0.38	0.09	0.05	0.01	0.05

2.2 Electrochemical studies

To carry out an electrochemical investigation, we employed a three-electrode cell: the WE (working electrode), with the CS surface has previously prepared, the RE (reference

electrode), which is based on the SCE and the CE (counter electrode), with platinum. The Tafel curves and impedance diagrams are provided by the "Voltamaster4" software computer, which is coupled to a potentiostat/galvanostat PGZ-100 that linked to the cell with a double-wall thermostat. To create a steady-state open circuit potential (OCP) for the various inhibitor concentrations, the working electrode must be stabilized and maintained in the solution for 30 minutes. the polarization curve plots were created while maintaining a scan rate of 0.5 mV/sec throughout a potential range of -800 to -200 mV. EIS diagrams were generated at OCP potential using an AC signal with an amplitude of 10 mV and a frequency range of (100 kHz - 10 mHz).

2.3 UV-Vis analysis

Ultraviolet-visible absorption spectrophotometry (UV-Visible has also been utilized to study the mechanism behind TzPz behavior with CS-substrate surfaces in 1M HCl environment.

Using the spectrophotometric technique, CS samples were submerged in HCl (1M) acid for three days at 303 K, either with or without the addition of an inhibitor TzPz at the optimum concentration 10^{-3}M. Measurements were performed with a Jasco V-730 UV/Visible spectrophotometer, under the control of Spectra Manager software. (200 – 800 nm) was the wavelength range that was investigated.

2.4 Quantum computing method DFT

The computing approach was applied to study the TzPz electronic characteristics order to predict a potential reactivity tendency of the tested molecule. To do this, a DFT calculation is performed with the B3LYP functional and the 6-31G(d,p) basis set, which is handled by the Gaussian (09W) 2013 program module, to get the reactivity descriptors. The quantum-chemical descriptors were calculated using formulas from earlier research.

3 Results and interpretation

3.1 PDP measurements

PDP curves for CS in 1M HCl media in reference & TzPz solutions is elucidated in Fig. 2. The deduced parameters from these curves for the various concentrations tested are regrouped in Table 2, namely current density, Tafel slopes, corrosion-potential (noted respectively: cathodic-β (βc), anodic-β (βa), i_{corr} and E_{corr}). Inhibitory effectiveness based on i_{corr} of each inhibitor was calculated by this Eq:

$$E_{Tafel}(\%) = \left(\frac{i_{cor,free} - i_{cor,Inh}}{i_{cor,free}}\right) \times 100 \quad (1)$$

where $i_{cor.free}$, $i_{cor.inh}$ are the densities current in uninhibited & inhibited solutions, respectively.

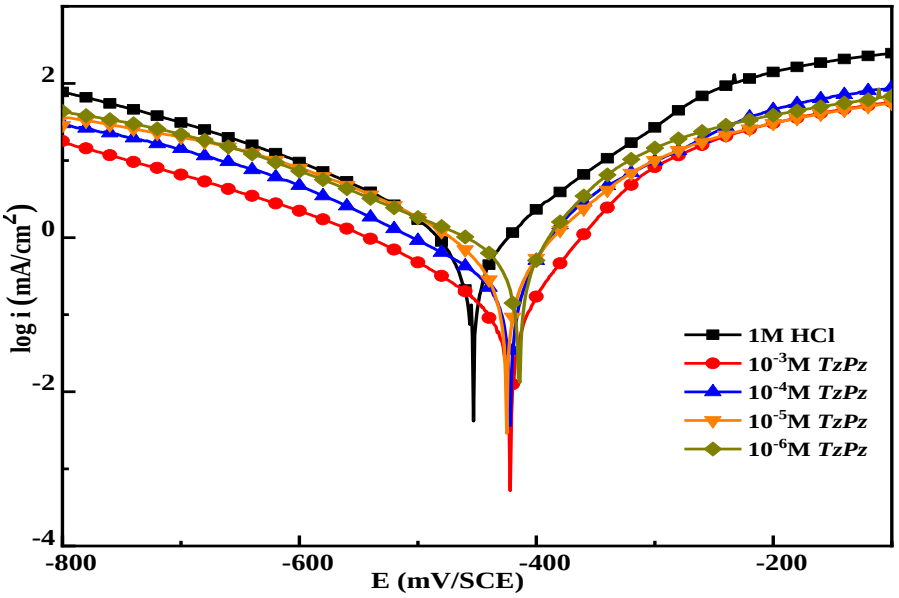

Fig.2. Tafel curves of M-steel uninhibited and inhibited with different concentrations of TzPz in used acid at 303 K.

Table 2 Data deducted from Tafel extrapolation of M-steel uninhibited and inhibited with various [C] of TzPz in 1M aggressive acid at 303 K.

Media	***Conc.***	***-E_{corr} (mV vs. SCE)***	***i_{corr} (μA cm^{-2})***	***Tafel slopes (mV dec^{-1})***		***η_{Tafel} (%)***
				$-\beta_c$	***β_a***	
Blank	1M	456.3	1104.1	112	155.4	---
TzPz	10^{-6}	415.5	420.7	102.4	56.3	61.9
	10^{-5}	425.4	229.2	119.9	62.9	79.2
	10^{-4}	422.2	167.8	123.0	60.5	84.8
	10^{-3}	421.7	89.4	133.1	63.1	**91.9**

Figure 2 illustrates that the progressive addition of TzPz resulted in a decrease in the current density of anodic and cathodic reactions for CS in comparison to the reference solution. demonstrating that adding an inhibitor to an acidic environment slows down the reduction of hydrogen and lessens the anodic dissolution of CS. Furthermore, cathodic branches gave rise to parallel Tafel droits, indicating that the addition of TzPz doesn't alter the hydrogen evolution processes[7] .It is primarily a charge transfer mechanism that reduces the hydrogen ions on the metallic surface.

The data deduced from extrapolating the PDP curves are listed in Table 2. It's clear that a decrease in the i_{corr} combined with an increase in the tested TzPz molecule's concentration results in an increase in η_{Tafel} (%), which reaches to 91.9%. This indicates that this substance functions as an efficient corrosion inhibitor of CS in HCl. Furthermore, E_{corr} (around 40.8

mV), which is less than 85 mV, did not show any detectable change, recommending that the investigated inhibitor functioned as mixed inhibitor that impacted the anodic & cathodic processes[8]. Based on the values of β_a and β_c (anodic and cathodic Tafel points), it appears that this system evolves by slowing down the corrosion process without changing the metal's dissolving mechanism[9].

3.2 EIS analysis

The electrochemical method (EIS) was applied To further explore TzPz's capacity to reduce the rate of corrosion on MS, a useful non-destructive technique that is frequently utilized in the corrosion domain is electrochemical impedance spectroscopy (EIS) [10-12], it enables the corrosion inhibition potential to be assessed by examining the interactions in the vicinity the acid solution/metal interface[13]. The mechanism of the electrochemical process and the phenomena of corrosion are closely related. The major focus of corrosion research is on the features of corrosion that take place at the interface between electrolyte / metal surface [14]. So, the system studied M-steel/solution of TzPz was handled using the EIS technique, which permits the charting of the Nyquist and Bode diagrams, following stabilization by immersion in solutions for 30 minutes.

A simple method to measure efficiency is to identify the polarization resistance, which is often estimated as the region encircled by the semicircle in Nyquist plots ($\eta Z(\%)$) according the following Eq(2) [15].

$$\eta_Z(\%) = \left(\frac{R_{p,Inh} - R_{p,free}}{R_{p,Inh}}\right) \times 100 \qquad (2)$$

The polarization resistance in inhibitor and reference solutions is denoted by $R_{P.inh}$ and $R_{P.free}$, respectively.

The Nyquist and Bode diagrams, generated from the EIS for CS submerged in a 1 M HCl solution without and with various doses of TzPz at 303 K are shown in Figs. 3 and 4.

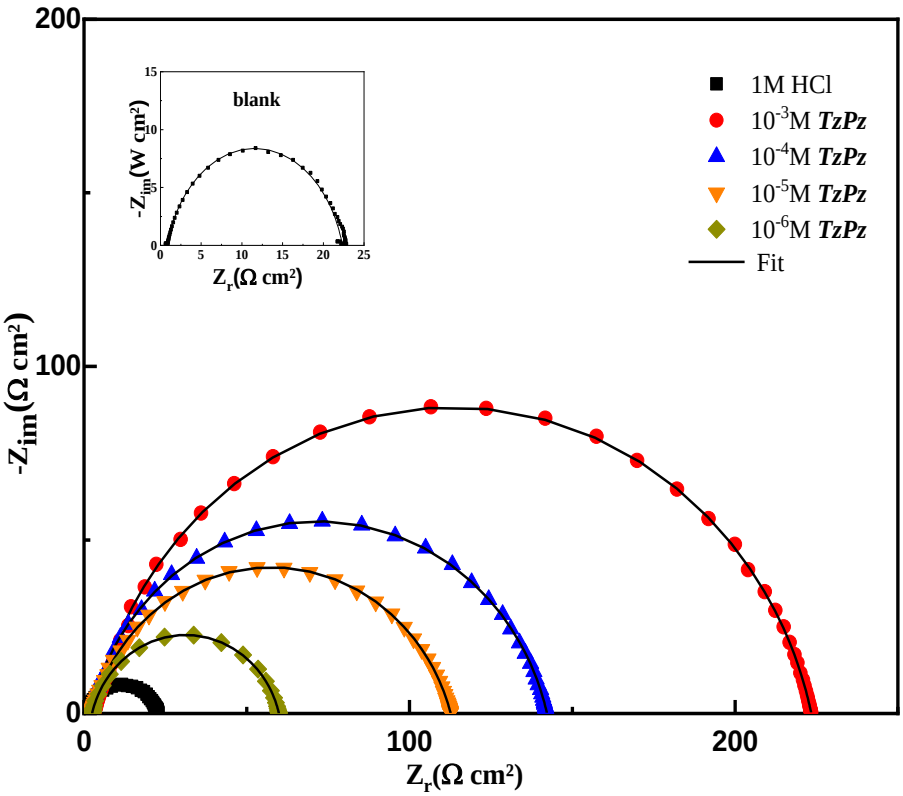

Fig.3. Nyquist diagrams for M-steel /1M HCl/ TzPz systems.

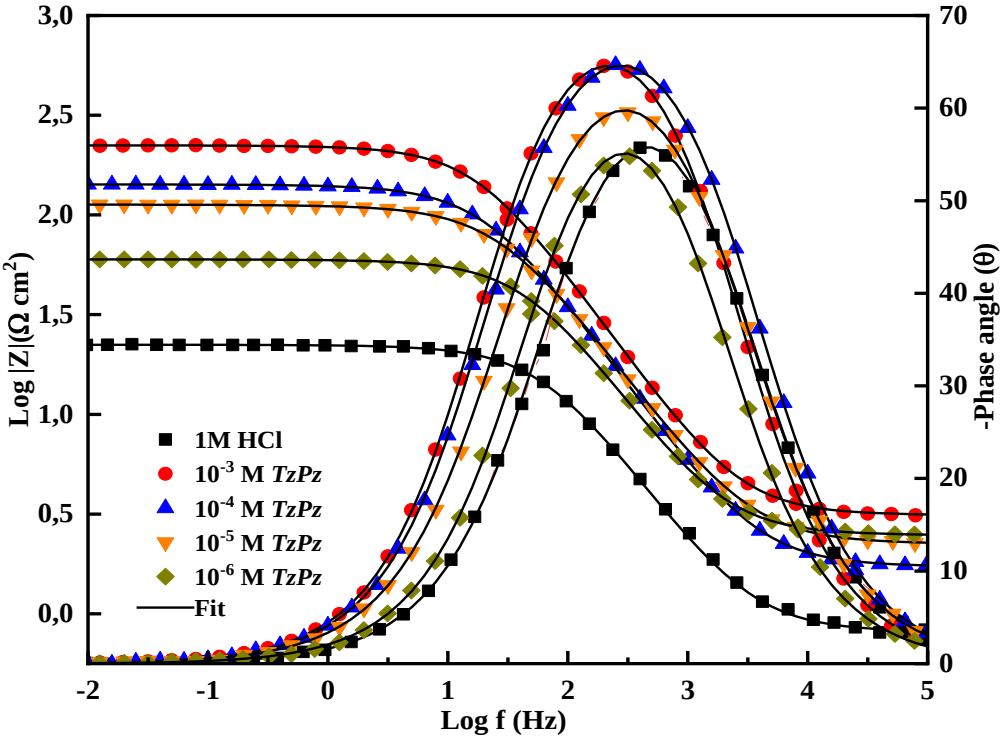

Fig.4. Bode-phase diagrams for M-steel/1M HCl/ *TzPz* systems.

The Nyquist diagrams in fig. 3 (which comprise of one depressed capacitive semi-circles) demonstrate that the corrosion process is unaffected by the TzPz presence [16]. Nonetheless, when the inhibitor concentration rises, the capacitive loop diameter increases. The Bode diagram in Figure 4 shows a single peak that corresponds to a single time constant, it exhibits the same behavior. The TzPz addition didn't cause a change in the semi-circular shape, indicating that the corrosion process is under charge transfer control and is unchanged[17].

The equivalent circuit utilized for fitting the impedance data is seen in (Figs. 5). The solution resistance and polarization resistance are represented, respectively, by R*s* and R*p* (which equal the sum of *Rct* and *Rf* which represents the resistance of the film created on the metal) and CPE represents the constant phase element. The double-layer capacitance (C_{dl}) was replaced with the CPE impedance in order to improve the EIS results from the experiment. Equations 3 and 4 provide definitions for this substitution:

$$Z_{CPE} = A^{-1}(i\omega)^{-1} \quad (3)$$

$$C_{dl} = \left(Q \times R_p^{1-n}\right)^{1/n} \quad (4)$$

where n, A, i, and ω represent the deviation index, the CPE constant, the imaginary number, and the angular frequency, respectively.

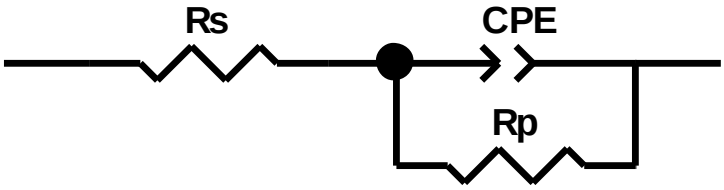

Fig.5. Equivalent circuit to simulate impedance spectra of system M-steel / inhibitors.

Table 3 EIS characteristics of M-steel corrosion in 1M HCl in absence & presence of TzPz.

Media	***Conc.***	R_s (Ω cm^2)	R_p (Ω cm^2)	C_{dl} (μF cm^{-2})	$10^6 \times A$ ($\Omega^{-1}s^{n-1}$ cm^{-2})	n_{dl}	χ^2	η_Z %
Blank	1M	0.8	21.57	116.2	293.9	0.853	0.002	-
TzPz	10^{-6}	2.4	57.3	60.9	142.2	0.85	0.008	**62.3**
	10^{-5}	2.2	110.4	56.9	128.4	0.84	0.007	**80.5**
	10^{-4}	1.7	140.6	53.8	112.0	0.85	0.008	**84.6**
	10^{-3}	3.0	220.3	39.7	77.2	0.86	0.009	**90.2**

The fitted EIS parameters for CS in 1 M HCl, both with and without TzPz at various [C] at 303K, are displayed in Table 2. Increased R_p results after the inhibitor addition when TzPz concentration rises from 10^{-6} to 10^{-3} M. This process is characterized by the creation of an inhibitor-adsorption film on the metal surface, which reduces the number of electroactive sites that are accessible for corrosion. This gives improved anti-corrosion effectiveness, with a maximum value of 90.2% at high inhibitor concentrations. Additionally, when the additive concentration rises, the C_{dl} values decrease which is accompanied by a decrease of *CPE,* the reason behind this may be attributed to the TzPz additive covering the surface of metal, which reduces the exposed area of the electrode face. The relaxation time (τ) is also dependent on the values of (C_{dl}), which can be found using the following formula.

$$\tau = \left(C_{dl} \times R_p\right) \quad (5)$$

Depending on the concentration of TzPz the relaxation time constant τ becomes more significant, which supports a delayed adsorption process time. It's also important to note that the suggested circuit is confirmed by the extremely low xi-square values (Table 3) in the studied concentration range. This implies that, in addition to the adsorption phenomena, there may be a blockage of the active sites that cause the dissolution of CS in the presence of TzPz. Both when the inhibitory molecule is present and absent, the values of n are strictly smaller than one, indicating an adsorption of TzPz at metallic surface as well as a surface irregularity. Additionally, this molecule may activate the bond formation with the vacant d-orbitals of Fe at the surface [18]. Furthermore, as stated in the literature, this phenomena is proof of the formation of the bond O-Fe, with distinctive donor-acceptor interactions between Fe unoccupied d-orbitals / electron pairs (sp^2) of the N-atoms in the triazole and pyrazole ring[19].

3.3 Isotherm model

Testing the TzPz adsorption model throughout the corrosion process is required to understand the inhibition mechanism of TzPz onto the mild steel surface in the inhibited medium. In order to model the link between inhibitor concentration/surface coverage, a variety of adsorption isotherm formulas, including Langmuir, Freundlich, and Temkin, have been investigated in this work utilizing the electrochemical spectroscopy impedance data.

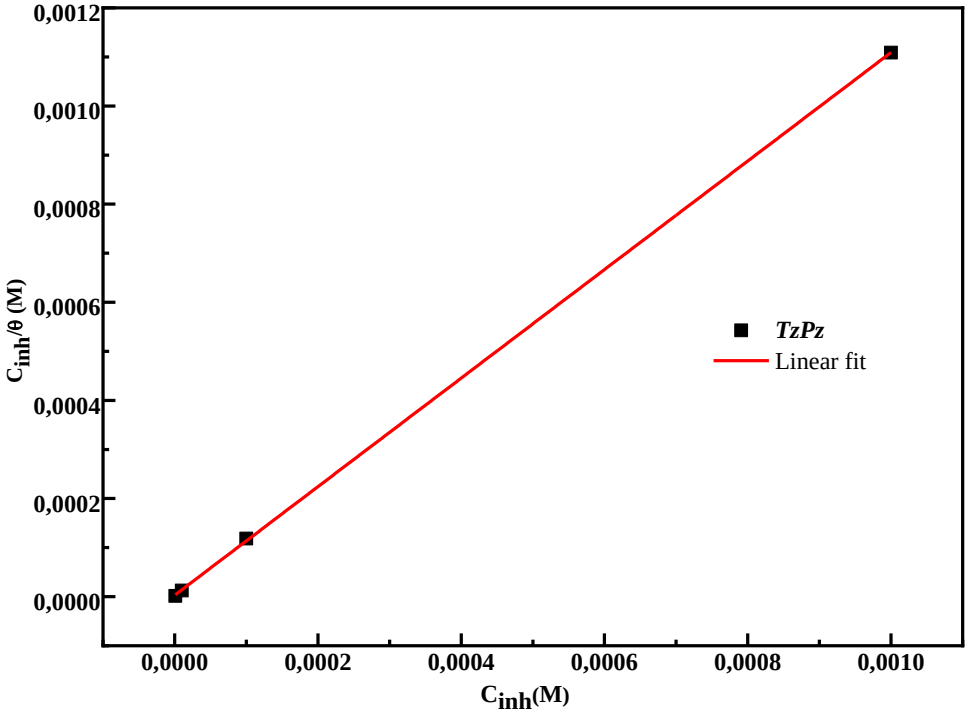

Fig.6. Langmuir isotherm for M-Steel in 1.0 M HCl medium at various concentrations of the inhibitor tested.

Table 4 Thermodynamic parameters for adsorption of TzPz on CS at 303 K.

	K_{ads} (L /mol)	ΔG_{ads} (KJ/mol)	Slope	R^2
TzPz	332755.4	-42.1	1.10608	0.999

The results indicate that the plot above presents a straight line, as seen in Fig. 6 and Table 4. because it achieves a slope that is almost equal to 1 (1.10) and the best regression coefficient (0.999). As a result, the inhibitor adsorption of the inhibitor on CS surface obeys to the Langmuir adsorption isotherm. The relatively high K_{ads} values indicate that our inhibitory molecule has a significant adsorption on the metal surface [20].

$$\frac{C}{\theta} = \frac{1}{K_{ads}} + C \quad (6)$$

where C is the inhibitor concentration and K_{ads} for the equilibrium constant.

The standard free energy of TzPz may be computed at different temperatures using the equation (7):

$$\Delta G^{\circ}_{ads} = -RT\,Ln(55.5K_{ads}) \quad (7)$$

where T (K) is the temperature, 55.5 is the water molar concentration (mol/L), and R (J $mol^{-1}K^{-1}$) is the universal gas constant.

According to existing literature [21, 22]a physical adsorption process is characterized by free energy values of about or less than −20 kJ mol^{-1}, whereas values of approximately or more than −40 kJ mol^{-1} indicate that the adsorption is primarily categorized as a chemisorption, and an intermediate value corresponding to a physico-chemical adsorption. The ΔG°_{ads} in our case is 42.1 kJ mol^{-1}, indicating that chemisorption interactions are implicated in the TzPz adsorption.

3.4 Temperature effect study

A number of industrial domains identify temperature as one of the elements that affects metal corrosion in acidic media by influencing the metal/inhibitor interaction[23, 24]. A good inhibitor should generally be stable, especially in acidic pickling solutions. To demonstrate this, the PDP technique was used to study the temperature effect on the corrosion inhibition of CS in 1.0 M HCl in the uninhibited and inhibited solutions of 10^{-3} M at temperatures ranging from 303 to 333 K. Table 5 lists the different electrochemical parameters, and Fig. 7 displays the polarization curves at the maximum tested concentration (10^{-3} M).

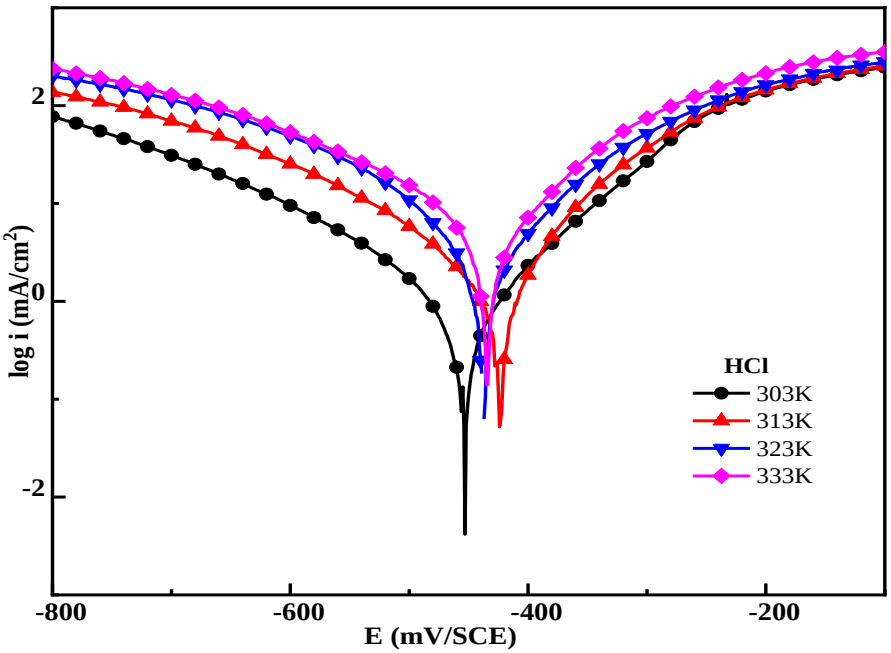

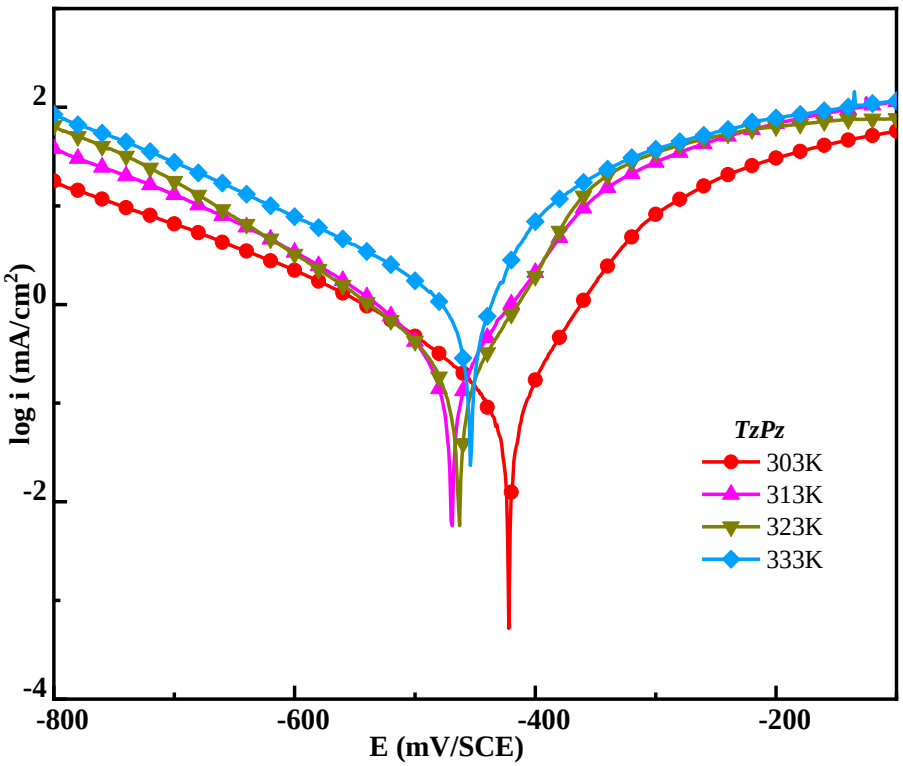

Fig.7. PDP curves for CS in 1M HCl containing different temperatures without and with the addition of 10^{-3}M TzPz.

Table 5 Electrochemical parameters and corrosion inhibiting effectiveness of CS in 1.0 M HCl without and with the addition of 10^{-3}M TzPz at different temperatures.

Medium	Temperature	$-E_{corr}$	i_{corr}	*Tafel slopes (mV dec^{-1})*		η_{PP}
	K	mV/SCE	μA cm^{-2}	$-\beta_c$	β_a	%
Blank	333	433.3	3944.9	134.6	103.9	-
	323	436.3	2254.0	117.8	91.4	-
	313	423.5	1477.4	131.3	91.3	-
	303	456.3	1104.1	112.8	155.4	-
TzPz.	333	452.6	884.8	156.7	61.5	**77.6**
	323	463.3	486.1	121.6	67.8	**78.4**
	313	467.2	220.7	101.5	76.6	**85.1**
	303	421.7	89.4	133.1	63.1	**91.9**

The temperature study reveals that the current density (i_{corr}) values in the presence of the investigated inhibitor are lower than those in (HCl), indicating that this ligand TzPz has significantly reduced the corrosion reaction of CS.

Table 5 shows that increasing the temperature from 303 to 333 K causes an increase in i_{corr} values from 89.4 to 884.8 μA cm^{-2}. Furthermore, the inhibitory efficiency diminishes marginally in the presence of the inhibitor TzPz, from 91.9% to 77.6%, indicating that this inhibitor is still effective against steel corrosion in aggressive solution (HCl). As a result, the studied compound still exhibits good inhibitory performance in protecting CS against corrosion by producing a solid adsorption film on metallic surface[25, 26] .

The graphs in Figs. 8 & 9 respectively, depict the Arrhenius plots of Ln(i_{corr}) vs. 1000/T and Ln(i_{corr}/T) vs. 1000/T of M-steel in 1.0 M HCl solution containing TzPz. Using the Arrhenius equation (8) and the transition state equation (9), the corrosion kinetic parameters, including activation energy (Ea) (which was obtained from linear square fits of ln i_{corr} *vs.* 1000/*T)*, activation enthalpy (ΔH_a**)** and activation entropy (ΔS_a) (which were acquired from linear square fits of ln i_{corr}/*T vs.* 1000/*T)* , were computed for the corrosion of CS in an acidic solution both without and with the TzPz inhibitor at the highest tested concentration (10^{-3} M) at temperatures between 303 & 333 K.

$$i_{corr} = Ae^{(\frac{-E_a}{RT})} \tag{8}$$

$$i_{corr} = \frac{RT}{Nh} e^{(\frac{\Delta S^*}{R})} e^{(\frac{\Delta H^*}{RT})} \tag{9}$$

The variables N, T, R, and $\hbar$ represent Avogadro's number, absolute temperature, gas constant, and Plank's constant, respectively.

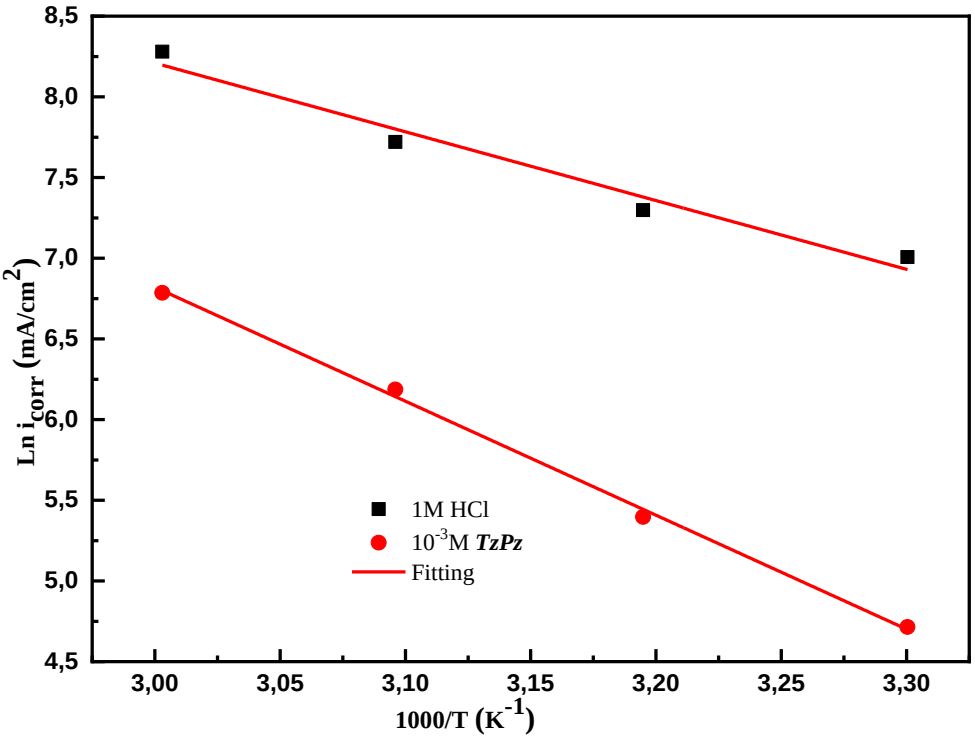

Fig.8. Arrhenius lines of CS in molar HCl medium in the absence & presence of TzPz.

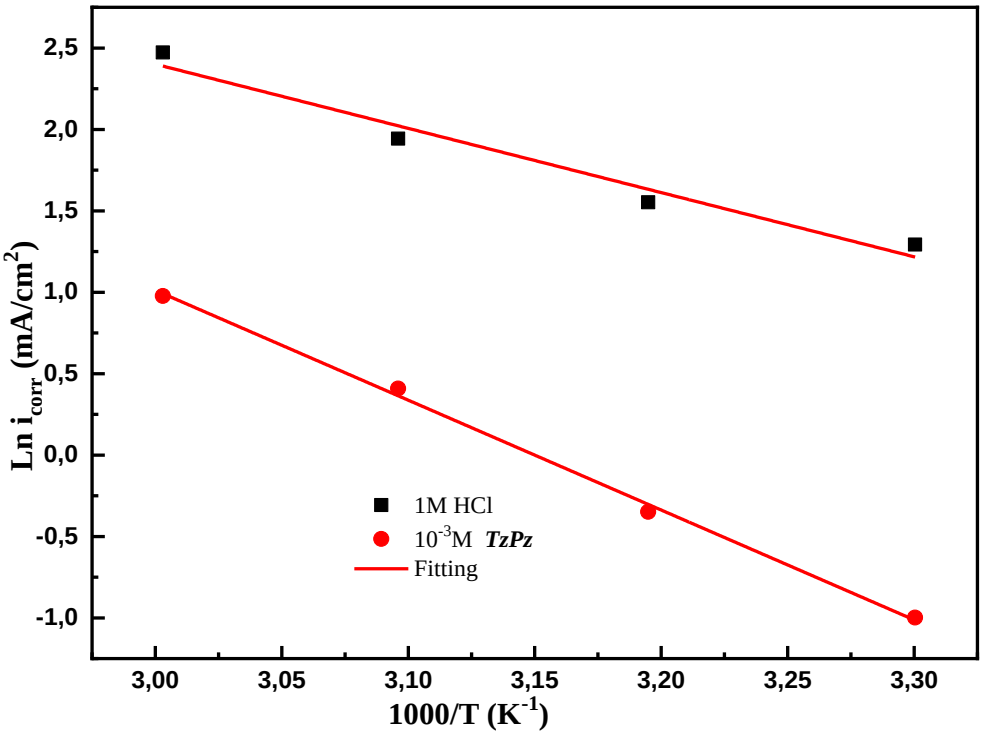

Fig.9. Arrhenius lines of Ln (i_{corr}/T) =f(1/T) for CS in aggressive HCl molar concentration in the absence and presence of TzPz.

Table 6 Activation parameters for the dissolution of CS in molar HCl without and with the TzPz presence.

Media	E_a (kJ/mol)	ΔH_a (kJ/mol)	ΔS_a (J/mol.K)
Blank	35.4	32.8	-79.2
TzPz	58.8	56.1	-20.9

Table 6 presents the activation parameters for MS in HCl with and without the exanimated triazole-pyrazole derivative. Based on the activation parameters values, it is evident that the solution containing TzPz has a larger E_a value (58.8KJ/mol) than the uninhibited solution (35.4 KJ/mol). This difference may be clarifying by the creation of a compact barrier film on the CS surface [27]. Inhibited solution has a larger energy barrier for corrosion, which implies that metal dissolution is reduced.

The positive activation enthalpy values demonstrate the endothermic character of CS dissolution process [28]. The increase in activation entropy value upon passage from the blank to the inhibitory solution indicates the passage of the barrier crossing towards TzPz adsorption on the MS surface[19]. The negative sign of activation entropy values indicates a

decrease in the disorder during the transformation of the reagents into an activated complex [29].

3.5 UV-Vis measurements

The objective of UV-Visible analysis of the 1M HCl solution with and without TzPz at the optimal concentration is to determine the inhibitor's complexing capability with ferrous ions. The UV–visible spectra in HCl before and after the addition of the inhibitor were carried out to confirm the possibility of the creation of a TzPz–Fe complex (Fig. 10). Two bonds are present at 211.11 nm as well as three peaks are present at 240.71-241.12 and 338.99 nm in the UV-visible spectra obtained both before and after immersion[30]. The absorption band peaks correspond to the π-π* transitions of the C=C bonds of the pyrazole ring [31]and the n-π* transition of the N=N groups of the triazole.

Addition of inhibitor caused a minor change in the maximum wavelength position (λmax) of the intense peak from 240.71nm to 241.12nm. These results show that the compound TzPz can bind to Fe^{2+} ions, hence the addition of our inhibitory molecule will most likely result in a complexation during the test, and can help reduce the amount of dissolved ferrous ions (Fe^{2+}) through the complexation process [32, 33].

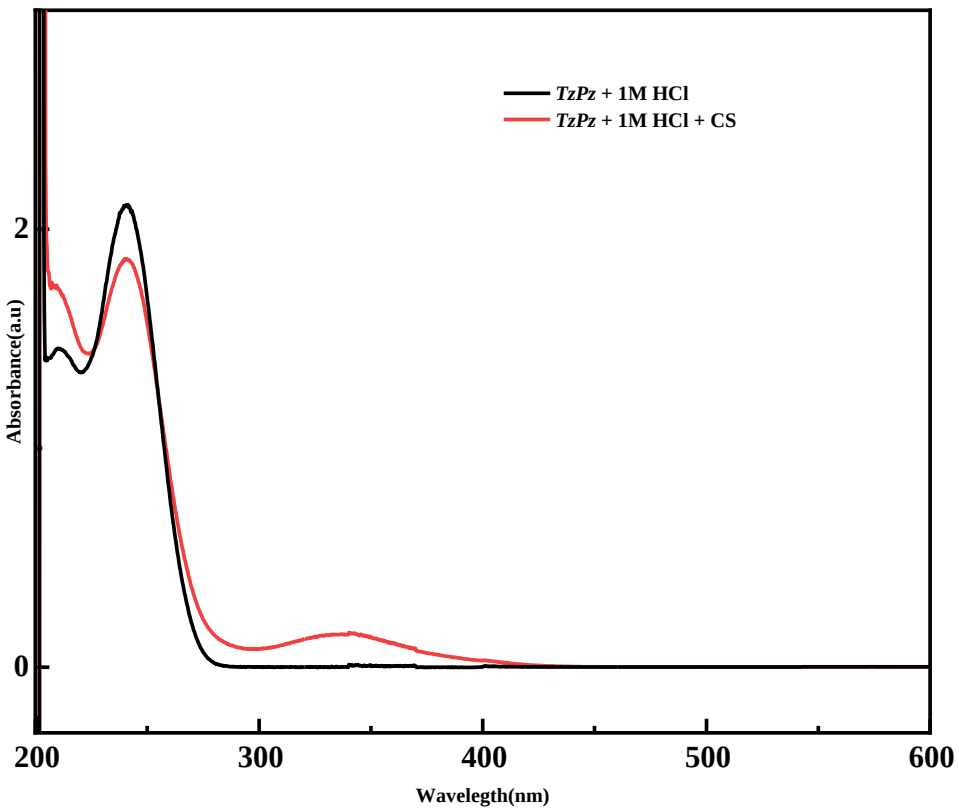

Fig.10. TzPz UV-vis spectra / HCl solution before and after soaking of CS.

3.6 Theoretical approach, DFT analysis

Theoretical simulations are essential for collecting a wide range of data on the inhibitory phenomena. The inhibition efficacy of inhibitor molecules is connected to the reactivity descriptors, which enable to comprehend the theoretical approach of this molecule and to better understand the interfacial processes of corrosion[16, 34, 35].
The neutral and protonated forms of molecular structure tested TzPz, have been optimized using the density functional theory method (DFT) and both forms are demonstrated in Figs.12 and 13. The main quantum chemical parameters such as HOMO (high occupied molecular orbital), LUMO (lowest unoccupied molecular orbital), ΔE (energy gap), σ (softness), (η) hardness, χ (electronegativity), and ΔN (fraction of electrons transferred) have been determined basing on Gaussian software (09W) and were collected in Table 6. These parameters play a significant role in the in prediction of the interaction between metallic surface and inhibitor molecule.

In HCl media, the tested TzPz molecule can protonate. To determine which atom(s) are more likely to bind the H^+ proton, all of the distributions of protonated forms as a function of pH (0 to 14) were shown using Marvin Sketch software [25]. The Fig.11 depicts the favorable location for protonation that was discovered to be accessible in the TzPz structure at site N8 with a percentage of 91.47 percent.

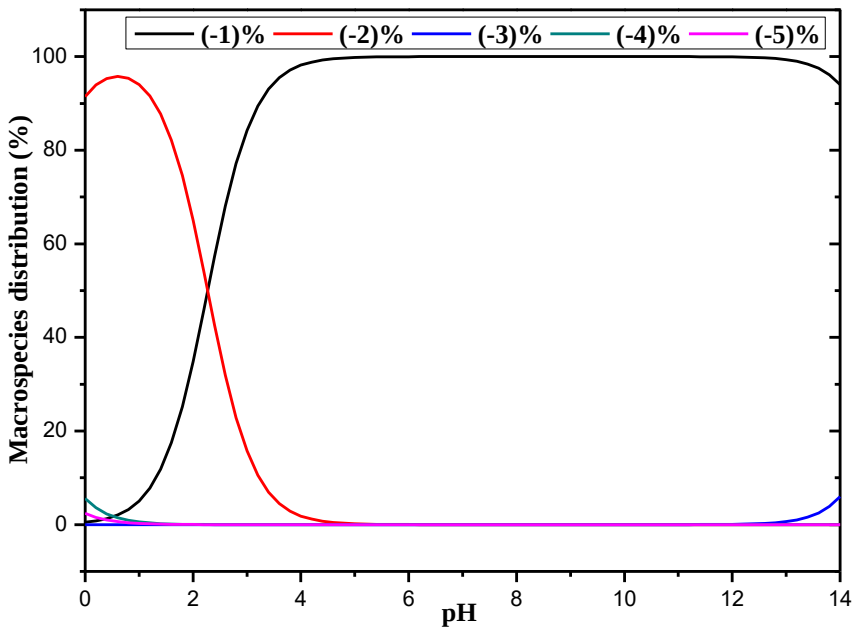

Fig.11. Microspecies distribution of protonated form of *TzPz (*% protonation vs. pH distribution).

Inhibitor **HOMO** **LUMO**

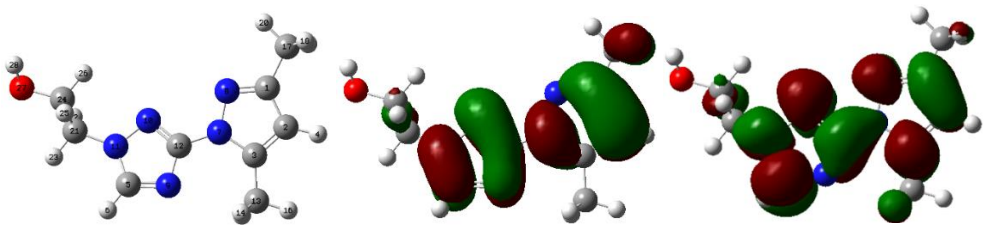

Fig.12. neutral molecule TzPz's optimized molecular structure and FMO (HOMO & LUMO).

Inhibitor **HOMO** **LUMO**

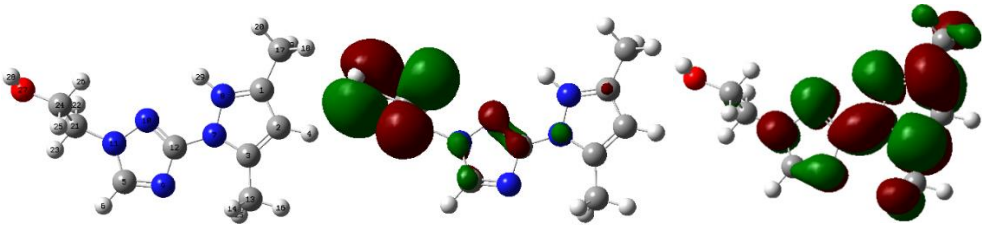

Fig.13. protoned molecule TzPz's optimized molecular structure and FMO (HOMO & LUMO).

Fig.14.

Table 7 Compututional parameters of *TzPz* neutral and protonated forms.

Descriptors	***Neutral form***	***Protonated form***
E_{HOMO}	-5.931	-10.302
E_{LUMO}	-0.184	-5.342
ΔE_{gap}	5.746	4.959
η (ev)	2.873	2.479
χ (ev)	3.058	7.822
ΔN_{110}	0.609	-1.214
μ (D)	2.3159	4.3775
E_T	-699.75	-700.145

According to FMO theory, the most quantum parameters are the highest energy of the occupied molecular orbital (E_{HOMO}) and the lowest unoccupied molecular orbital energy (E_{LUMO}). They determine the capability of the donor-acceptor interactions respectively, between the metal surface and the corrosion inhibitor. Thus, a high HOMO value suggests that the inhibiting molecules have a preference for offering electrons to Fe orbitals that are vacant on the metallic surface, whereas a low E_{LUMO} value suggests that the inhibiting

molecules have the ability to accept electrons from the Fe surface through retro-donation[36]. Therefore, an inhibitor molecule that exhibits low E_{LUMO} and high E_{HOMO} values is more effective in preventing corrosion.

The two orbitals for the neutral form of the molecule TzPz, HOMO and LUMO, are more concentrated on the rings of triazole and pyrazole, as shown in fig.12. This suggests that nitrogen atoms are the preferable locations for electrophilic assaults on the surface CS. Furthermore, Figure 13. illustrates that the LUMO orbital is centered on the identical skeleton in the protonated form (the triazole and pyrazole rings). Conversely, the HOMO electron density is distributed on the remaining part (ethan-1-ol) of the TzPz.

Table 7 demonstrates that the neutral form's high E_{HOMO} value suggests that it donates more electrons than the protonated form does. Further evidence that the protonated molecule cannot release electrons comes from the negative ΔN value in the protonated state. A low value of ΔE_{gap} and a large dipole moment (μ) represent the global molecular reactivity. This is obviously seen in our case; therefore, the protonated form is more reactive than the neutral form.

4 Conclusion

In conclusion, our study presents the evaluation of a new compound, ethyl 2-(3-(3,5-dimethyl-1H-pyrazol-1-yl)-1H-1,2,4-triazol-1-yl) ethan-1-ol (TzPz), as a corrosion inhibitor for CS in 1 M HCl. Through various spectroscopic methods, we confirmed the compound's structure and demonstrated its impressive inhibitory efficiency of 91.9% at 10^{-3} M concentration. Our investigation identified the OH substituent and Triazole-Pyrazole rings as pivotal contributors to this heightened corrosion inhibition effect.

Moreover, EIS results revealed that the corrosion process is primarily controlled by charge transfer with a single time constant. in the presence of TzPz, the resistance values Rp rise while the capacity Cdl decrease due to adsorption of the studied molecule on the metal surface. PDP curves demonstrated the inhibitory molecule is of mixed type. While thermodynamic analysis elucidated the inhibitor's operation through both chemisorption and physisorption mechanisms. Additionally, UV/Vis spectrophotometry confirmed the formation of a ligand–metal complex. The congruence between our theoretical simulations and experimental results further bolsters the validity of our conclusions.

References

1. Chkirate, K., et al., *Solvent induced supramolecular polymorphism in Cu (II) coordination complex built from 1, 2, 4-triazolo [1, 5-a] pyrimidine: Crystal structures and anti-oxidant activity.* Journal of Inorganic Biochemistry, 2020. **208**: p. 111092.
2. Askari, M., et al., *Downhole corrosion inhibitors for oil and gas production–a review.* Applied Surface Science Advances, 2021. **6**: p. 100128.
3. Alibakhshi, E., et al., *Glycyrrhiza glabra leaves extract as a green corrosion inhibitor for mild steel in 1 M hydrochloric acid solution: experimental, molecular dynamics, Monte Carlo and quantum mechanics study.* Journal of Molecular Liquids, 2018. **255**: p. 185-198.
4. Ramezanzadeh, M., et al., *Studying the Urtica dioica leaves extract inhibition effect on the mild steel corrosion in 1 M HCl solution: Complementary experimental, ab initio quantum mechanics, Monte Carlo and molecular dynamics studies.* J. Mol. Liq., 2018. **272**: p. 120-136.
5. Zhang, H., et al., *Inhibition performance of halogen-substituted benzaldehyde thiosemicarbazones as corrosion inhibitors for mild steel in hydrochloric acid solution.* RSC advances, 2022. **12**(47): p. 30611-30625.
6. Sedik, A., et al., *Dardagan Fruit extract as eco-friendly corrosion inhibitor for mild steel in 1 M HCl: Electrochemical and surface morphological studies.* Journal of the Taiwan Institute of Chemical Engineers, 2020. **107**: p. 189-200.
7. Khattabi, M., et al., *Performance and computational studies of two soluble pyran derivatives as corrosion inhibitors for mild steel in HCl.* Journal of Molecular Structure, 2019. **1196**: p. 231-244.
8. Fouda, A., et al., *Evaluation of 4-amidinophenyl-2, 2′-bithiophene and its aza-analogue as novel corrosion inhibitors for CS in acidic media: experimental and theoretical study.* Journal of Molecular Liquids, 2017. **240**: p. 372-388.
9. Biswas, A., et al., *Grafting effect of gum acacia on mild steel corrosion in acidic medium: Gravimetric and electrochemical study.* Journal of Molecular Liquids, 2018. **251**: p. 470-479.
10. Abdulazeez, I., et al., *Mechanistic studies of the influence of halogen substituents on the corrosion inhibitive efficiency of selected imidazole molecules: a synergistic computational and experimental approach.* Applied Surface Science, 2019. **471**: p. 494-505.
11. Aslam, R., et al., *A comprehensive review of corrosion inhibitors employed to mitigate stainless steel corrosion in different environments.* Journal of Molecular Liquids, 2022: p. 119992.
12. Azzaoui, K., et al., *Eco friendly green inhibitor Gum Arabic (GA) for the corrosion control of mild steel in hydrochloric acid medium.* Corrosion Science, 2017. **129**: p. 70-81.
13. Elyoussfi, A., et al., *The effect of functional groups on the inhibitory efficacy of newly synthesized Imidazopyridines compounds against the corrosion of mild steel in acidic environments: Electrochemical, thermodynamic, surface and computational investigations (Part B).* Journal of Molecular Structure, 2023: p. 136025.
14. Elyoussfi, A., et al., *Some quinoline derivatives: Synthesis and comparative study towards corrosion of mild steel in 0.5 MH2so4.* Der Pharma Chemica, 2016. **8**(4): p. 226-236.

15. Salhi, A., et al., *A correlated theoretical and electrochemical investigation of the corrosion inhibition performance of phenolic Schiff bases on mild steel in HCl solution (Part B).* Inorganic Chemistry Communications, 2023: p. 110684.
16. Verma, C., et al., *An overview on plant extracts as environmental sustainable and green corrosion inhibitors for metals and alloys in aggressive corrosive media.* Journal of molecular liquids, 2018. **266**: p. 577-590.
17. Fernandes, C.M., et al., *Green synthesis of 1-benzyl-4-phenyl-1H-1, 2, 3-triazole, its application as corrosion inhibitor for mild steel in acidic medium and new approach of classical electrochemical analyses.* Corrosion Science, 2019. **149**: p. 185-194.
18. Berrissoul, A., et al., *Assessment of corrosion inhibition performance of origanum compactum extract for mild steel in 1 M HCl: Weight loss, electrochemical, SEM/EDX, XPS, DFT and molecular dynamic simulation.* Industrial Crops and Products, 2022. **187**: p. 115310.
19. Hassouni, H.E., et al., *Corrosion inhibition, surface adsorption and computational studies of new sustainable and green inhibitor for mild steel in acidic medium.* Inorg. Chem. Commun., 2022. **143**: p. 109801.
20. Al-Azawi, K.F., et al., *Experimental and quantum chemical simulations on the corrosion inhibition of mild steel by 3-((5-(3, 5-dinitrophenyl)-1, 3, 4-thiadiazol-2-yl) imino) indolin-2-one.* Results in Physics, 2018. **9**: p. 278-283.
21. Kıcır, N., et al., *Investigation of ammonium (2, 4-dimethylphenyl)-dithiocarbamate as a new, effective corrosion inhibitor for mild steel.* Corrosion Science, 2016. **105**: p. 88-99.
22. Mobin, M., S. Zehra, and R. Aslam, *L-Phenylalanine methyl ester hydrochloride as a green corrosion inhibitor for mild steel in hydrochloric acid solution and the effect of surfactant additive.* RSC advances, 2016. **6**(7): p. 5890-5902.
23. Kaya, S., et al., *Determination of corrosion inhibition effects of amino acids: quantum chemical and molecular dynamic simulation study.* Journal of the Taiwan Institute of Chemical Engineers, 2016. **58**: p. 528-535.
24. Zarei, A., et al., *Pepper extract effectiveness as a natural inhibitor against corrosion of steel samples (SS) in 1 M hydrochloric acid; Theoretical (DFT calculation–MD simulation), thermodynamic, and electrochemical-surface studies.* Ind Crops Prod . 2022. **189**: p. 115839.
25. Zhang, H.-h., X. Pang, and K. Gao, *Effect of surface roughness on the performance of thioureido imidozaline inhibitor in CO2-saturated brine.* Corrosion Science, 2019. **157**: p. 189-204.
26. Hamani, H., et al., *1-(4-Nitrophenylo-imino)-1-(phenylhydrazono)-propan-2-one as corrosion inhibitor for mild steel in 1 M HCl solution: weight loss, electrochemical, thermodynamic and quantum chemical studies.* Journal of Electroanalytical Chemistry, 2017. **801**: p. 425-438.
27. Ech-Chihbi, E., et al., *Experimental and computational studies on the inhibition performance of the organic compound "2-phenylimidazo [1, 2-a] pyrimidine-3-carbaldehyde" against the corrosion of carbon steel in 1.0 M HCl solution.* Surfaces and Interfaces, 2017. **9**: p. 206-217.
28. El Hezzat, M., et al., *Correlated DFT and electrochemical study on inhibition behavior of ethyl 6-amino-5-cyano-2-methyl-4-(p-tolyl)-4H-pyran-3-carboxylate for the corrosion of mild steel in HCl.* Der Pharma Chem, 2015. **7**(10): p. 77-88.
29. Yadav, M., et al., *Experimental and quantum chemical studies of synthesized triazine derivatives as an efficient corrosion inhibitor for N80 steel in acidic medium.* Journal of Molecular Liquids, 2015. **212**: p. 151-167.

30. Hrimla, M., et al., *Corrosion inhibition performance of a structurally well-defined 1, 2, 3-triazole derivative on mild steel-hydrochloric acid interface.* Journal of Molecular Structure, 2021. **1231**: p. 129895.
31. Abboud, Y., et al., *2, 3-Quinoxalinedione as a novel corrosion inhibitor for mild steel in 1 M HCl.* Materials chemistry and physics, 2007. **105**(1): p. 1-5.
32. Zhang, W., et al., *Halogen-substituted acridines as highly effective corrosion inhibitors for mild steel in acid medium.* The Journal of Physical Chemistry C, 2018. **122**(44): p. 25349-25364.
33. Erami, R.S., et al., *Carboxamide derivatives as new corrosion inhibitors for mild steel protection in hydrochloric acid solution.* Corrosion Science, 2019. **151**: p. 190-197.
34. Soltani, N., et al., *Green approach to corrosion inhibition of 304 stainless steel in hydrochloric acid solution by the extract of Salvia officinalis leaves.* Corros. Sci., 2012. **62**: p. 122-135.
35. El Basiony, N., et al., *Retard the corrosion reaction of carbon steel in acid solutions using Gemini-nonionic surfactant: Theoretical and experimental studies.* Materials Today Communications, 2023. **37**: p. 107378.
36. Jawad, Q., et al., *Synthesis and comparative study of novel triazole derived as corrosion inhibitor of mild steel in hcl medium complemented with dft calculations.* International Journal of Corrosion and Scale Inhibition, 2020. **9**(2): p. 688-705.